Prediction of Complex Two-Dimensional Trajectories by a Cerebellar Model of Smooth Pursuit Eye Movement

R. E. KETTNER,[1] S. MAHAMUD,[2] H.-C. LEUNG,[1] N. SITKOFF,[2] J. C. HOUK,[1] B. W. PETERSON,[1] AND A. G. BARTO[2]

[1]*Department of Physiology M211, Northwestern University Medical School, Chicago, Illinois 60611; and*
[2]*Department of Computer Science, University of Massachusetts, Amherst, Massachusetts 01003*

Kettner, R. E., S. Mahamud, H.-C. Leung, N. Sitkoff, J. C. Houk, B. W. Peterson, and A. G. Barto. Prediction of complex two-dimensional trajectories by a cerebellar model of smooth pursuit eye movement. *J. Neurophysiol.* 77: 2115–2130, 1997. A neural network model based on the anatomy and physiology of the cerebellum is presented that can generate both simple and complex predictive pursuit, while also responding in a feedback mode to visual perturbations from an ongoing trajectory. The model allows the prediction of complex movements by adding two features that are not present in other pursuit models: an array of inputs distributed over a range of physiologically justified delays, and a novel, biologically plausible learning rule that generated changes in synaptic strengths in response to retinal slip errors that arrive after long delays. To directly test the model, its output was compared with the behavior of monkeys tracking the same trajectories. There was a close correspondence between model and monkey performance. Complex target trajectories were created by summing two or three sinusoidal components of different frequencies along horizontal and/or vertical axes. Both the model and the monkeys were able to track these complex sum-of-sines trajectories with small phase delays that averaged 8 and 20 ms in magnitude, respectively. Both the model and the monkeys showed a consistent relationship between the high- and low-frequency components of pursuit: high-frequency components were tracked with small phase lags, whereas low-frequency components were tracked with phase leads. The model was also trained to track targets moving along a circular trajectory with infrequent right-angle perturbations that moved the target along a circle meridian. Before the perturbation, the model tracked the target with very small phase differences that averaged 5 ms. After the perturbation, the model overshot the target while continuing along the expected nonperturbed circular trajectory for 80 ms, before it moved toward the new perturbed trajectory. Monkeys showed similar behaviors with an average phase difference of 3 ms during circular pursuit, followed by a perturbation response after 90 ms. In both cases, the delays required to process visual information were much longer than delays associated with nonperturbed circular and sum-of-sines pursuit. This suggests that both the model and the eye make short-term predictions about future events to compensate for visual feedback delays in receiving information about the direction of a target moving along a changing trajectory. In addition, both the eye and the model can adjust to abrupt changes in target direction on the basis of visual feedback, but do so after significant processing delays.

INTRODUCTION

Smooth pursuit eye tracking is highly accurate, and several studies have shown that eye movements can actually predict the future course of simple target motions. For example, when a visual target is moved back and forth at a constant frequency, the eye soon locks onto the target so that there is little or no lag, and sometimes even a slight lead, between eye and target. This has been shown during tracking of a variety of periodic stimuli, including sine and square waves in one dimension (Bahill and McDonald 1983; Dallos and Jones 1963; Kowler and Steinman 1979; Lisberger et al. 1981; Pola and Wyatt 1980) and circular and rhomboid trajectories in two dimensions (Collewijn and Tamminga 1984; Deno et al. 1995; Leung and Kettner 1997). This tracking behavior is considered predictive because visual signals are processed by the smooth pursuit system with considerable delays that have been estimated at ~100 ms (Becker and Fuchs 1984; Carl and Gellman 1986; Fuchs 1967; Leung and Kettner 1997; Lisberger and Westbrook 1985; Robinson 1965). One would expect tracking to lag by similar delays during smooth pursuit if the eye were controlled exclusively by a simple negative feedback system based on visual input.

Complex trajectories created by summing sinusoids can also be tracked with various degrees of predictive control. Although sum-of-sines stimuli have often been used in an attempt to create ''random'' and therefore ''unpredictable'' target trajectories, some investigators (e.g., Dallos and Jones 1963; Yasui and Young 1984) have shown that low-frequency components of these sum-of-sines trajectories can be tracked with phase leads that suggest predictive control. Barnes et al. (1987) have stressed that the highest-frequency component of a sum-of-sines waveform can be tracked with high gains and small phase lags that also indicate predictive control. We have recently extended these results to complex, two-dimensional pursuit for the monkey (Kettner et al. 1996); low-frequency sinusoidal components were tracked with consistent phase leads, whereas middle- and high-frequency components were tracked with very small phase lags. To verify that these monkeys were tracking predictively, we computed visual processing delays in response to perturbations from circular pursuit and compared these delays with tracking delays during complex two-dimensional sum-of-sines pursuit in the same monkeys (Leung and Kettner 1997). The lag between eye and target during circular pursuit before the perturbations averaged 3 ms. This value was much smaller than the 90-ms average delay in responding to right-angle perturbations from this circular trajectory. Similarly, the average delay during complex sum-of-sines pursuit was 20 ms, much smaller than the time required to process visual information.

0022-3077/97 $5.00

Both the sum-of-sines and circle-with-perturbation results provide interesting challenges for models of pursuit. The excellent short-lag tracking behavior observed for sum-of-sines trajectories requires a model of pursuit that can generate complex predictive control. In addition, the circle-with-perturbation data confirm that visual information is also used to guide the tracking of unexpected target motions when predictive control is not possible. This means that complete models should allow predictive and feedback control to work in concert to generate the full range of smooth pursuit behaviors. In addition, an ultimate model of the neural control of pursuit should be biologically plausible. Most previous models of smooth pursuit have addressed only its feedback control component (Deno et al. 1995; Krauzlis and Lisberger 1989; Robinson et al. 1986; Young et al. 1968). These models are typically couched in the form of linear system operations, which do not explicitly incorporate features of the neural pathways that generate smooth pursuit. In an attempt to generate predictive tracking of complex target motions, Van den Berg (1988) and Barnes and Asselman (1991) have suggested that the pursuit system has a buffer that stores target motions. Performance of such models is limited by the length of the buffer, and it is not immediately apparent how they would be implemented by known neural circuits involved in pursuit.

Here we present a neural network model based on the anatomy and physiology of the flocculus and paraflocculus of the cerebellum, brain areas that have been related to the control of smooth pursuit eye movements (Zee et al. 1981). The model can generate complex predictive smooth pursuit while still mediating responses to unexpected perturbations, which require feedback control. This is the first model that generates complex predictive pursuit with the use of an explicit simulation of control processing implemented by a biologically reasonable architecture. This model represents an extension of our previous models of limb movement control, which have been constrained by the anatomy and physiology of the intermediate cerebellum (Berthier et al. 1993; Houk and Barto 1992; Houk et al. 1990). As in recent renditions of the limb model (Barto et al. 1996; Buckingham et al. 1995), we utilize a learning rule with an ''eligibility trace'' and incorporate the rich diversity of mossy fiber input to the cerebellum. The eligibility trace allows delayed feedback of errors to modify the strength of connections that were active at the time at which the motor commands that led to the error were generated (Houk and Alford 1996; Klopf 1972, 1982; Sutton and Barto 1981). The inclusion of diverse mossy fiber inputs together with a granular layer creates a sparse expansive recoding of these inputs that is well suited for associative mapping (Albus 1971; Marr 1969; Tyrrell and Willshaw 1992). The simulated mossy fiber inputs are based on the behavior of actual neurons revealed by single-neuron recording studies (Lisberger and Fuchs 1978a,b; Maekawa and Kimura 1980; Miles et al. 1980; Mustari et al. 1988; Stone and Lisberger 1990a,b; Suzuki et al. 1990). These various features allow the model to learn to generate predictive pursuit despite the fact that pursuit error signals are delayed by 100 ms. Unlike the limb control model, which regulates state transitions in Purkinje cells, the present model generates continuous outputs that control smooth eye movements.

In outline, the paper first describes our cerebellar model in mathematical detail while at the same time justifying with physiological data the choices made in formulating the mathematical equations and in selecting the model parameters. Results from simulations of the model are then presented and compared with analogous data obtained from behaving monkeys studied in our laboratory. All of these findings are integrated with the existing literature in a final discussion. The monkey results used to test the model have been reported in more detail elsewhere. Monkey tracking behavior and estimates of component interactions during complex two-dimensional sum-of-sines pursuit are presented in Kettner et al. (1996). Leung and Kettner (1997) describe pursuit behavior during right-angle perturbations from circular pursuit, as well as quantifying predictive control during complex pursuit with comparisons between visual feedback delays and tracking delays during complex pursuit. Preliminary reports of the model have also appeared (Kettner et al. 1995; Mahamud 1995; Mahamud et al. 1996).

Model

The structure of the network model is shown in terms of the neuronal architecture of the cerebellum in Fig. 1 and functionally in Fig. 2. Information enters the network via 440 pathways representing mossy fibers. Of these, some mossy fibers conveyed two-dimensional visual information about the position ($n = 40$) and velocity ($n = 40$) of the target image on the retina, and other mossy fibers provided information related to the position ($n = 180$) and velocity ($n = 180$) of the eye relative to the head. In each case, information was conveyed with time delays spanning ranges that are realistic for each population of mossy fibers. We denote the activation of mossy fiber i at time t by $m_i(t)$, $i = 1, \ldots, 440$.

Retinal position error was coded by 40 visual mossy fibers (8 preferred position directions $\times$ 5 delays ranging from 80 to 120 ms in 10-ms steps). Similarly, retinal velocity error was conveyed by 40 fibers (8 preferred velocity directions $\times$ 5 delays ranging from 80 to 120 ms). In both cases, preferred directions ranged from 0 to 315° at intervals of 45°. Specifically, let $\mathbf{e}(t)$ denote the two-dimensional retinal position error vector at time t, which is the vector difference between the retinal target image and the center of view (the fovea) at time t (bold type indicates that a quantity is a vector); let $\mathbf{n}_i$ denote the unit vector in the preferred direction of mossy fiber i; and let τ_i denote the delay by which mossy fiber i transmits information to the cerebellum. Then the activation of retinal position error mossy fiber i, $i = 1, \ldots, 40$, at time t, is

$$m_i(t) = \max\,[\mathbf{n}_i \cdot \mathbf{e}(t - \tau_i)/e_{\max}, 0] \qquad (1)$$

where $e_{\max}$ is the maximum expected magnitude of $\mathbf{e}(t)$ used to normalize $m_i(t)$. The centered dot indicates the inner, or scalar, product of the two vectors. Taking the maximum of the normalized inner product and 0 ensures that the mossy fiber activation is never negative. Similarly, the activation of retinal velocity error mossy fiber i, $i = 41, \ldots, 80$, is

$$m_i(t) = \max\,[\mathbf{n}_i \cdot \dot{\mathbf{e}}(t - \tau_i)/\dot{e}_{\max}, 0] \qquad (2)$$

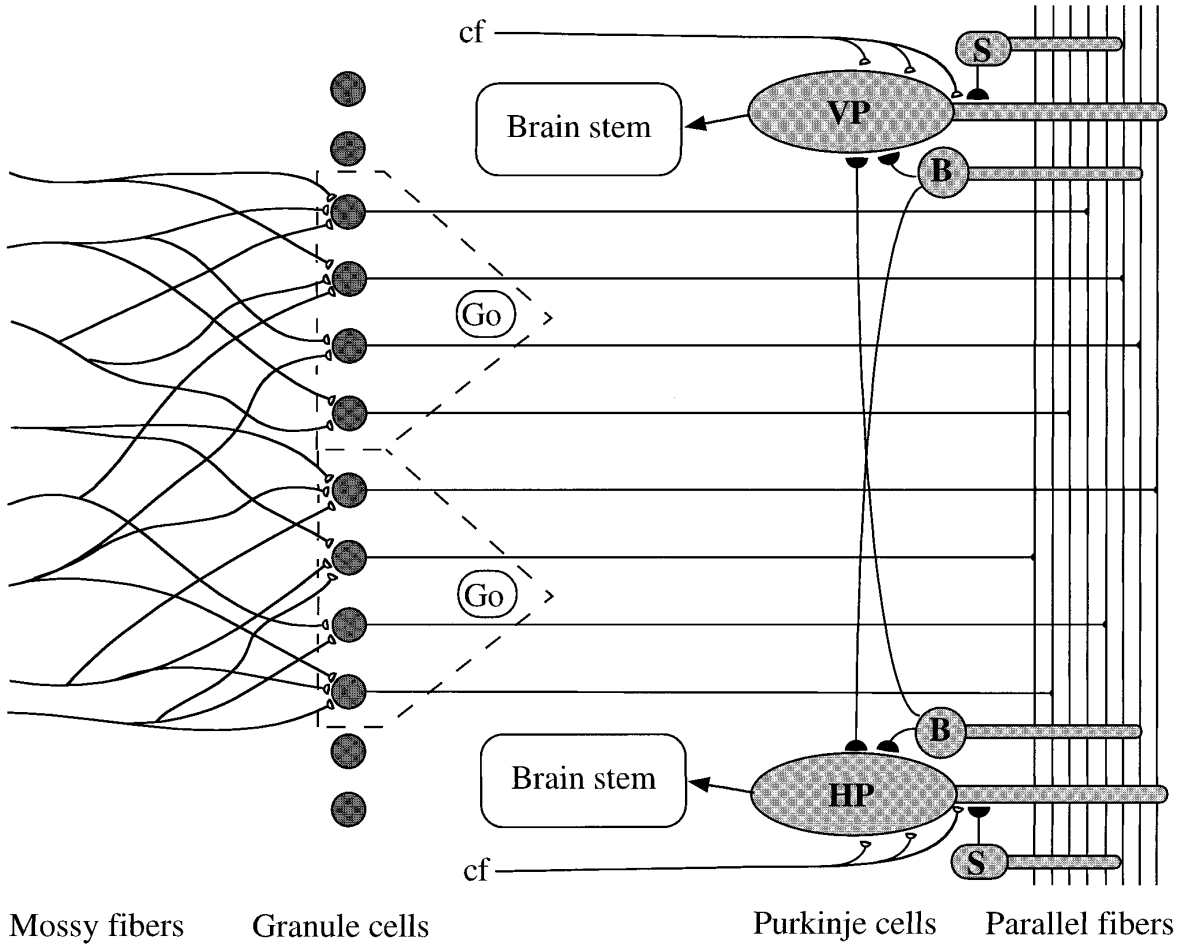

FIG. 1. Architecture of the cerebellar model. Mossy fibers are randomly connected to granule units. Dotted lines: hypothesized influence of Golgi cell (Go) receptive fields that allow only those granule cells with the highest activity to generate outputs. Axons from granule cells bifurcate into 2 parallel fibers that excite horizontal (HP) and vertical (VP) Purkinje units. Basket (B) and stellate (S) units receive excitatory parallel fiber input and inhibit Purkinje cells. The action of these unit types is collapsed into ''Purkinje units'' that allow both positive and negative ''parallel fiber'' weights. Climbing fiber (cf) inputs are used to train the network.

where $\dot{\mathbf{e}}(t)$, the time derivative of $\mathbf{e}(t)$, is the retinal velocity error vector, and $\dot{e}_{\max}$ is the maximum expected magnitude of $\dot{\mathbf{e}}(t)$.

This approximates the broad cosine spatial tuning (Fig. 3*A*) that has been observed experimentally (Mustari et al. 1988; Suzuki et al. 1990) for neurons in the dorsolateral pontine nucleus, which provides visual input to the cerebellum. The distribution of visual delays is derived from single-neuron recordings in the dorsolateral pontine nucleus (Mustari et al. 1988; Suzuki et al. 1990) and the cerebellar flocculus/paraflocculus (Miles et al. 1980).

The second set of mossy fiber inputs provides signals related to eye movement at biologically realistic delays. Eye position is coded by 180 mossy fibers (4 preferred position directions $\times$ 3 thresholds $\times$ 3 slopes $\times$ 5 delays ranging from 0 to 40 ms in steps of 10 ms), and eye velocity is coded by 180 additional mossy fibers (4 preferred velocity directions $\times$ 3 thresholds $\times$ 3 slopes $\times$ 5 delays from 0 to 40 ms). These signals are based on responses from granular layer input units recorded from the cerebellar flocculus/paraflocculus (Lisberger and Fuchs 1978a,b; Miles et al. 1980) and have preferred directions aligned with either the vertical or horizontal axes in four directions (up, down, right, left). Because of their relatively short delays, these signals are likely to arise from brain stem systems that either provide an efference copy of motor commands or are driven by proprioceptive inputs (Maekawa and Kimura 1980).

Mathematically, the activation levels of eye position mossy fibers, which are the mossy fibers *i*, $i = 81, \ldots, 260$, are defined as follows

$$m_i(t) = \max \{\mathbf{n}_i \cdot [\mathbf{a}_i + b_i \mathbf{x}(t - \tau_i)]/x_{\max}, 0\} \quad (3)$$

where $\mathbf{n}_i$ is the unit vector in the fiber's preferred direction, $\mathbf{x}(t - \tau_i)$ is the eye position vector delayed by τ_i ms, $x_{\max}$ is the maximum expected magnitude of $\mathbf{x}(t)$ used to normalize $m_i(t)$, and the parameters $\mathbf{a}_i$ and b_i serve to diversify the response properties of the mossy fibers. Specifically, $\mathbf{a}_i$ is a vector whose two components determine response thresholds of mossy fiber *i* for horizontal and vertical eye position. For any mossy fiber *i*, we defined these components to both equal 0, 1/2, or 1. The scalar b_i, which determines the response slope of mossy fiber *i*, was set to 1/4, 1/2, or 3/4. These values were chosen so that all combinations occurred with approximately equal frequencies across the population

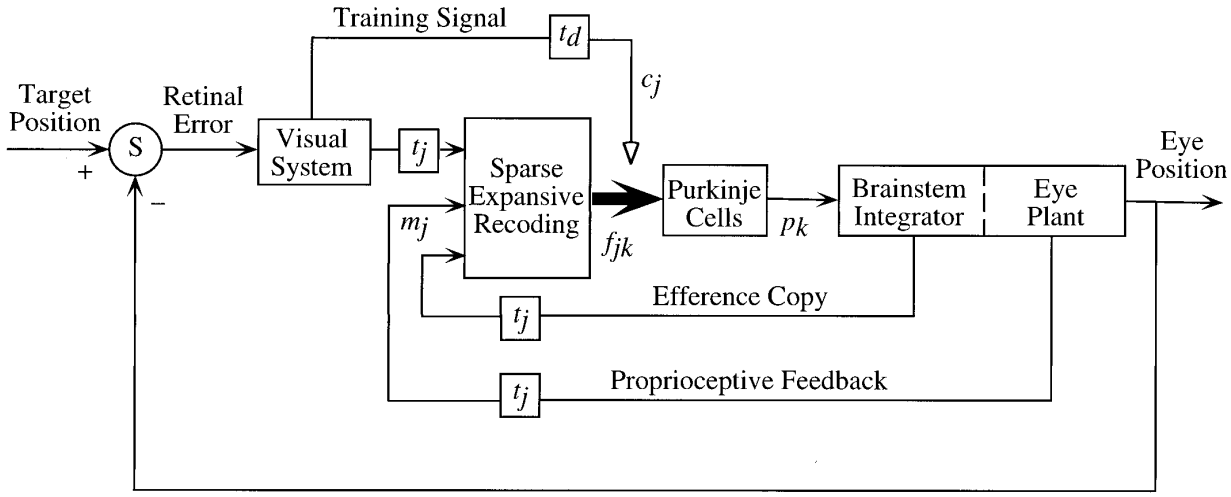

FIG. 2. Block diagram of the model. Although the brain stem integrator and the eye plant are modeled by the same set of equations in the model, these 2 functions are distinguished in the diagram to emphasize their different neural substrates and the idea that both proprioceptive and efference copy signals may provide eye position and velocity information. All lines indicate the flow of multivariate information, with the heavier arrow indicating the wider bandwidth associated with the expansive recoding of mossy inputs. Smaller boxes: pure delays in the model. Open arrowhead: indirect action climbing fiber training signals have on information throughput by the alteration of network weights via the learning rule. Visual input to the system is assumed to take the form of retinal error signals that are obtained by a subtraction at the node labeled S of target and eye position signals.

of mossy fibers. Examples of these linear response functions for one of the four preferred directions are illustrated in Fig. 3*B*. The activations of the 180 eye velocity mossy fibers i, $i = 261, \ldots, 440$, were defined as in *Eq. 3*, but with the delayed eye velocity vector, $\dot{\mathbf{x}}(t - \tau_i)$, substituted for the delayed eye position vector, $\mathbf{x}(t - \tau_i)$, and normalized by the maximum expected eye velocity magnitude.

Each of 6,000 granule units sums inputs from five randomly selected mossy fibers (Ito 1984; Palkovits et al. 1972). If for each j, $j = 1, \ldots, 6{,}000$, R_j is a set of (indexes of) 5 mossy fibers selected randomly (uniformly without replacement) from the total of 440 mossy fibers, then the activation of granule unit j at time t is

$$g_j(t) = \sum_{i \in R_j} h_i m_i(t) \tag{4}$$

The constants, h_i, were selected randomly from the interval (0.75, 1.00) at the beginning of a simulation and then remain fixed.

In deriving a pattern of parallel fiber activity from granule unit activations, we assumed that a local competition takes place that allows only 5% of the granule units to be active at any given time. Thus the continuous-valued mossy fiber activation pattern is recoded into a sparsely activated higher-dimensional vector of binary-valued parallel fiber activity that improves pattern discrimination, storage capacity, and learning (Tyrrell and Willshaw 1992). Marr (1969) and Albus (1971) assumed that this competition arose from inhibitory interactions by Golgi cells. To reduce computation times, we implemented this competition by dividing the granule cell population into 300 Golgi cell receptive fields each comprising 20 granule units, and allowed only the most active unit in each field to provide an output of 1 during any time step. Let G_j denote the set of (indexes of) the granule cells making up the Golgi cell receptive field in which granule cell j is located. Then the activation of parallel fiber j, $j = 1, \ldots, 6{,}000$, at time t is

$$f_j(t) = \begin{cases} 1 & \text{if } g_j(t) = \max_{n \in G_j} [g_n(t)] \\ 0 & \text{otherwise} \end{cases} \tag{5}$$

This results in 300 granule cells having an activity of 1, and the remaining 5,700 granule cells having an activity of 0. During the next simulated time step, granule cell activity is recomputed on the basis of new mossy fiber inputs. In practice, however, only a subset of the 300 active granule cells change state from one time step to the next.

Two units representing Purkinje cells generate horizontal and vertical movement commands in agreement with experimental reports that Purkinje cells fire primarily in relation to horizontal and vertical eye movement (Miles et al. 1980; Stone and Lisberger 1990a). In the brain, granule cell axons generate parallel fibers that excite Purkinje cells, as well as exciting basket and stellate cells that in turn inhibit Purkinje cells. This part of the cerebellar circuitry was modeled by defining the activation of the Purkinje unit k at time t, $p_k(t)$, to be a weighted sum of the activations at time t of all the model's parallel fibers

$$p_k(t) = p_o + \sum_{j=1}^{6{,}000} w_{jk}(t) f_j(t) \tag{6}$$

where $w_{jk}(t)$ represents the weight, or efficacy, of the synapse by which parallel fiber j influences Purkinje cell k, $k = 1{,}2$, and p_o is the Purkinje unit background firing rate. The parallel-fiber-to-Purkinje-unit weights were allowed to assume both positive and negative values to simulate the combined direct positive activation via parallel fiber input and indirect negative activation via basket and stellate cells. This assumption, made for the sake of computational simplicity, has been used in other cerebellar models (Fujita

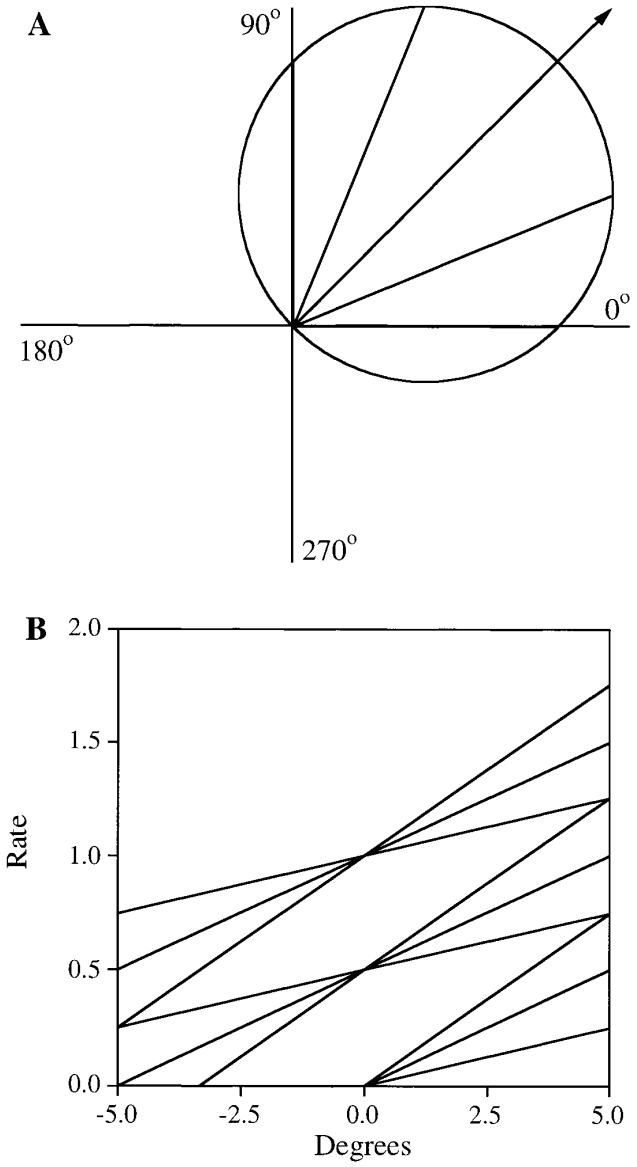

FIG. 3. Examples of mossy fiber response properties. *A*: visual mossy fibers had cosine tuning functions with a single preferred direction. In this figure firing rate was equal to the distance from the origin to the tuning function in the direction of target motion. Here the preferred direction of the mossy fiber was 45°. *B*: eye movement mossy fibers were tuned for horizontal and vertical movements with a variety of different slopes and thresholds. The figure shows the 9 different sets of tuning curves associated with rightward movement.

1982a,b) and is justified mathematically by assuming that each weight, *w*, is the combination of an excitatory weight w^+ and a negative weight w^- so that $w = w^+ - w^-$. Thus a positive synaptic weight corresponds to greater activation along the excitatory than the inhibitory pathway ($w^+ > w^-$), and a negative synaptic weight is associated with the opposite: greater activation along the inhibitory than the excitatory path ($w^- > w^+$). Changes in total weight, *w*, can correspond to changes in either the w^+ pathway alone, the w^- pathway alone, or a combination of both.

Outputs from the two Purkinje units generate horizontal and vertical eye movements via a model of the oculomotor plant that includes a neural integrator. Mathematically, this is accomplished in the simulation by the following two vector difference equations

$$\dot{\mathbf{x}}(t) = 0.41\,[\mathbf{p}(t) - \mathbf{p}_0] + 0.61\dot{\mathbf{x}}(t - \Delta t) \quad (7)$$

$$\mathbf{x}(t) = \mathbf{x}(t - \Delta t) + \dot{\mathbf{x}}(t)\Delta t \quad (8)$$

where $\mathbf{p}(t)$ is the vector of Purkinje unit activities at time *t,* and $\mathbf{p}_0$ is the vector of background firing rates. These equations were derived from the second-order linear equation relating average motoneuron firing rate, $\mathbf{s}(t)$, with eye position, **x,** due to Keller (1973)

$$\mathbf{s}(t) = \mathbf{s}_0 + 4.0\mathbf{x}(t) + 0.95\dot{\mathbf{x}}(t) + 0.015\ddot{\mathbf{x}}(t) \quad (9)$$

It is assumed that brain stem circuits account for the background firing rate, $\mathbf{s}_0$, and the position term, $4.0\mathbf{x}(t)$, via circuits that include a neural integrator (see review by Fukushima et al. 1992). Details of how this integration might be implemented by brain networks have been presented elsewhere (e.g., Anastasio and Robinson 1989; Arnold and Robinson 1991). The other two terms in the equation were assumed to relate to Purkinje unit output by the equation

$$\mathbf{p}(t) - \mathbf{p}_0 = 0.95\dot{\mathbf{x}}(t) + 0.015\ddot{\mathbf{x}}(t) \quad (10)$$

This equation was solved for $\dot{\mathbf{x}}(t)$ by substituting $\ddot{\mathbf{x}}(t) = [\dot{\mathbf{x}}(t) - \dot{\mathbf{x}}(t - \Delta t)]/\Delta t$ to derive *Eq. 7,* and $\mathbf{x}(t)$ was then obtained by integrating $\dot{\mathbf{x}}(t)$.

On the basis of experimental results (Leung and Kettner 1997; Robinson 1965), large tracking errors were corrected by catch-up saccades that stepped the eye to the location of the target. Saccades were initiated 200 ms after retinal position error exceeded 0.25°, followed by a refractory period of 200 ms during which saccades were not allowed to occur. When the retinal error exceeded 0.25° during the refractory period, a saccade was initiated at the end of this period. This meant that corrective saccades were always separated by ≥200 ms. We assumed that saccades were generated by other brain systems outside of the cerebellum. Several explicit models of saccade generation exist (e.g., Arai et al. 1994; Lefevre and Galiana 1992), and we did not attempt to duplicate this work. Saccades were more frequent during the early stages of training and declined in magnitude and frequency as the network learned.

Learning in the model takes the form of changes in the synaptic weights, w_{jk}, by which the parallel fibers influence Purkinje units. These weights change when a retinal velocity error (retinal slip) occurs in an appropriate temporal relationship with parallel fiber activation. Retinal velocity errors are sensed by the climbing fiber system and relayed to Purkinje units with a delay, *d,* that was set to 100 ms (Stone and Lisberger 1990b). The model adopts the hypothesis of Klopf (1972, 1982) of a synaptic eligibility trace that allows changes to be made in the weights of the synapses that were active ~100 ms before each climbing fiber signal arrived at a Purkinje unit. The eligibility trace is a temporary memory trace, local to the synapse, that is initiated whenever the presynaptic parallel fiber is active. It makes the synapse ''eligible'' for being modified if, and when, a climbing fiber signal arrives at the postsynaptic Purkinje unit within a time window of several hundred milliseconds (see Fig. 4). This allows changes in these synaptic weights of Purkinje units

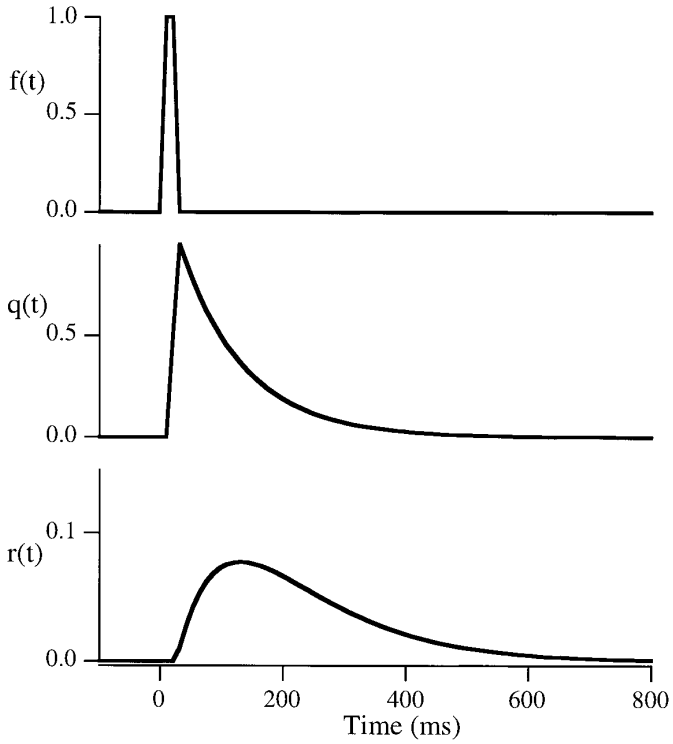

FIG. 4. Eligibility trace activation is broad with a peak at a delay of ~100 ms. In response to a step input from the parallel fiber input, f(t), the concentration of q(t) increases abruptly and then decays. These increases in q(t) then cause increases in the eligibility trace, r(t).

whose activity participated in causing the error conveyed by the climbing fiber.

Although there are a number of ways to produce an eligibility trace, we selected a biologically reasonable mechanism based on slow ''second-messenger'' chemical processes that are postulated to underlie synaptic change in cerebellar neurons (see DISCUSSION). The model generates the time courses of the eligibility trace, $r_{jk}(t)$, by the following coupled first-order linear difference equations

$$q_{jk}(t + \Delta t) = (1 - \beta)q_{jk}(t) + \gamma f_j(t) \quad (11)$$

$$r_{jk}(t + \Delta t) = (1 - \delta)r_{jk}(t) + \epsilon q_{jk}(t) \quad (12)$$

where the parameters β, γ, δ, and ϵ are all positive fractions. These equations provide a discrete time model of a series coupling of two ''leaky integrators.'' The time courses of r and q in response to a brief pulse input f are illustrated in Fig. 4. *Equation 11* implies that the cellular factor $q_{jk}(t)$ rises immediately in response to an increase in parallel fiber activity, $f_j(t)$, and otherwise decays toward 0. As elaborated in the DISCUSSION, we think of $q_{jk}(t)$ as the level of the protein kinase C (PKC) within the cell, the parameter γ as representing the rate at which glutamate released by parallel fiber activity leads to increases in PKC via metabotropic glutamate receptors, and β as the rate of spontaneous inactivation of PKC. Similarly, *Eq. 12* causes the eligibility trace level, $r_{jk}(t)$, to rise in response to increases in $q_{jk}(t)$ and to decay toward 0 otherwise. Here, we think of $r_{jk}(t)$ as the level of phosphorylation of α-amino-3-hydroxy-5-methyl-4-isoxazolepropionic acid (AMPA) receptors for glutamate, ϵ as the rate at which PKC levels promote this phosphorylation, and δ as the rate at which other enzymes dephosphorylate the receptors. With appropriate selection of these parameters ($\beta = 0.1$, $\gamma = 0.1$, $\delta = 0.1$, and $\epsilon = 0.1$) the synapse's eligibility level, $r_{jk}(t)$, rises to a peak ~100 ms after activation of the parallel fiber input and then declines (see Fig. 4).

A more abstract eligibility trace modeled as a pure delay, $\tilde{d}$, was used in some simulations to study the effects of the trace delay on learning. The result was an eligibility trace, $\tilde{r}_{jk}(t)$, defined simply by

$$\tilde{r}_{jk}(t) = f_j(t - \tilde{d}) \quad (13)$$

When $\tilde{d}$ was set equal to the climbing fiber delay, d, this trace produced excellent results for all trajectories in about half the simulated time steps required with the use of the trace defined by *Eqs. 11* and *12*. We used it in runs designed to study the effects of varying the trace delay (Fig. 8), and also to reduce computation times in the simulations that generated quantitative gain and phase data (Fig. 6). The trace defined by *Eqs. 11* and *12* was used to generate the simulation data presented in Figs. 5 and 7; very similar results were obtained with the use of *Eq. 13.*

The rising and falling eligibility level of a synapse provides one factor that influences synaptic weight changes; a second factor is activation of the climbing fiber. We model this process by the following rule for changing synaptic weights

$$\Delta w_{jk}(t) = -\alpha r_{jk}(t)[c_k(t) - c_o] \quad (14)$$

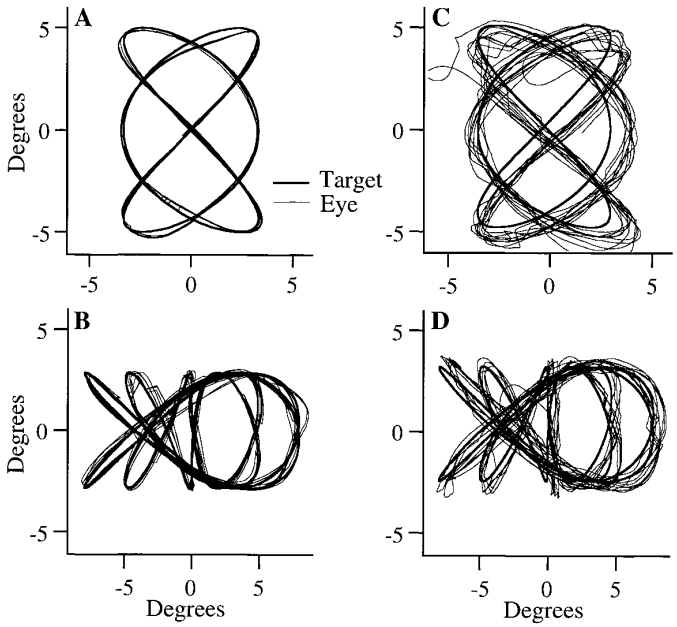

FIG. 5. Comparisons between model tracking (*left*) and monkey eye tracking (*right*) along complex trajectories. Heavy lines: target trajectories. Fine lines: tracking traces. *A* and *C*: tracking along H3V2 trajectories generated by combining horizontal (0.9 Hz, 3.33°) and vertical (0.6 Hz, 5°) sinusoids at 3 and 2 times the 0.3-Hz waveform frequency. *B* and *D*: tracking along H4H6V7 trajectories created by pairing 2 sinusoids at 4 and 6 times the 0.15-Hz waveform frequency on the horizontal axis (0.6 Hz, 5°; 0.9 Hz, 3.33°) with a 3rd sinusoid at 7 times the waveform frequency (1.05 Hz, 2.86°) on the vertical axis. Amplitudes were adjusted so that components had the same peak velocity.

where α is a parameter influencing the rate of learning, $r_{jk}(t)$ is the synapse's eligibility level, c_o is the background firing rate of the climbing fiber, and $c_k(t)$ is the climbing fiber's discharge rate defined by

$$c_k(t) = c_o + \mathbf{n}_k \cdot \dot{\mathbf{e}}(t - d) \quad (15)$$

Here, $\mathbf{n}_k$ is a unit vector in the preferred direction of the horizontal or vertical Purkinje unit and $\dot{\mathbf{e}}(t - d)$ is the retinal velocity error at time $t - d$, where d is the climbing fiber delay of 100 ms described above. In the simulations reported below, α ranged from 0.0001 to 0.00001, and $\tilde{r}_{jk}(t)$ replaced $r_{jk}(t)$ when the eligibility trace defined by *Eq. 13* was used. The very low values of α needed for successful learning by the model, which uses a continuous representation of the climbing fiber signal, may correspond to the low rates of climbing fiber discharge observed physiologically (Ito 1984).

We can summarize the behavior of the learning rule given by *Eq. 14* as follows. For a given Purkinje unit, whenever its climbing fiber is firing above or below its background rate, the weight of each of its parallel fiber synapses is changed by an amount that depends on *1*) the amount by which the climbing fiber's current activity differs from its background rate, *2*) the current eligibility level of the synapse, and *3*) the parameter α. A synapse's eligibility level is high to the extent that the synapse was active ~100 ms in the past. Climbing fiber activity deviates from its background rate to the extent that the target image was moving on the retina 100 ms in the past. Consequently, the learning rule selectively changes weights at those synapses that were active when retinal velocity errors occurred. In this way a set of weights is obtained that allows accurate target tracking by the network.

METHODS

The complex sum-of-sines stimuli used to test the model were identical to a subset of stimuli previously used to study monkey performance (Kettner et al. 1996). Complex trajectories were created by combining two or three sinusoids equated for velocity along horizontal and/or vertical axes (see Fig. 5). Model and monkey pursuit performance was quantified by fitting sinusoids at component frequencies to target and eye velocity traces with the use of a least-squares regression procedure. Regions of these traces containing saccadic jumps were deleted with the use of custom computer programs, and the regressions were then based on the remaining data. Gain was defined as the ratio of eye and target velocity amplitudes; phase was the phase difference in milliseconds between eye and target. This analysis produced three gain/phase pairs for each of the three components associated with tracking along a sum-of-three-sines trajectory, and two gain/phase pairs for pursuit along sum-of-two-sines or circular trajectories. This analysis is mathematically equivalent to estimating the discrete Fourier components at component frequencies on the basis of records with missing data (Press et al. 1992).

In a different set of simulations, the model was trained to track trajectories (see Fig. 7) that had previously been used to study perturbation responses in monkeys (see Leung and Kettner 1997). These trajectories consisted of three cycles of circular target motion followed by a right-angle perturbation along a circle meridian during the fourth cycle. This four-cycle sequence was repeated ≥10 times for both the model and the monkey to evaluate response patterns that were consistent across repetitions of the perturbation. Quantitative estimates of visual feedback delays for both the model and the monkeys were based on the first smooth deviation from the circular trajectory after the perturbation had begun. A custom computer program first subtracted the eye position during the unperturbed cycle just before the perturbation from the eye position during the perturbed cycle. This subtraction created a ''difference trace'' that eliminated systematic deviations from the target trajectory during normal pursuit. A regression line was then fit to the difference trace for a 50-ms period that began 25 ms before the perturbation. Only those records that were free from saccades during the perturbation were used in our analyses, as verified by viewing trace records of eye position and velocity. The latency of smooth corrections for a session was defined as the time after the perturbation of the first deviation from the regression line that was maintained for 100 ms. In a related fashion, the latency of saccadic corrections was defined as the first occurrence of a single deviation of 40°/s in velocity difference records.

The model was trained afresh on each stimulus from the initial state defined in the description of the model, until we observed good tracking with a minimum of corrective saccades and no performance improvement with additional training. All the results described in this paper are based on asymptotic performance of this sort. Although model training could require several days of computer time, the simulated time required to reach performance asymptote ranged from 8 to 33 min depending on the trajectory being trained and the eligibility rule that was used. Model performance typically reached asymptote after 100,000 simulated 10-ms time steps for the sum-of-two-sines (H3H2 and H3V2) waveforms, and after 200,000 time steps for the sum-of-three-sines (H4H6V7) and circles-with-perturbation trajectories, with the use of the eligibility trace defined by *Eqs. 11* and *12* with the optimal delay of 100 ms. This corresponded to 300 waveform presentations in each case, because the H3V2 and H2H3 waveforms had a repetition period of 3.33 s, which was half the repetition period of 6.67 s associated with the H4H6V7 and circles-with-perturbation waveforms. Training reached asymptote in about half the number of simulated time steps for the pure delay trace described by *Eq. 13.* Each model simulation was implemented in the C programming language running on DEC 5000 workstations, and required ~24 h to execute 50,000 simulated 10-ms time steps. No systematic attempt was made to study the effects of varying learning rate parameters or to optimize other model parameters, and it is likely that learning would have occurred more rapidly for a different set of model parameters.

We attempted to use similar training procedures for the model and the monkey, but the large times required to train the model necessitated several compromises. The first simplification was the elimination of waveforms that were 90° rotations of each other. Although the monkey results indicate clear differences in horizontal and vertical pursuit (Kettner et al. 1996), no such differences were built into this initial version of the model. Second, the model simulations presented here were based on training for a single waveform, whereas each monkey was tested on all of the pursuit stimuli as well as several other waveform trajectories. In addition, the monkey was continually pursuing targets in the home cage between experiments. These differences in the stimulus sets processed by the model and the monkey are likely to explain many of the small performance differences that were observed.

Standard methods were used to collect pursuit data from monkeys tracking complex two-dimensional trajectories. These techniques have been reported in detail elsewhere (Kettner et al. 1996), as will techniques for collecting data during perturbations from circular pursuit. Only a few key features of these experimental methods are described here. Two male rhesus monkeys were housed and maintained according to Guiding Principles in the Care and Use of Animals of the American Physiological Society. Care was taken to ensure the comfort of the animals during the experiment, and their general well being. An eye coil and stainless steel

cylinder for head fixation were surgically implanted under deep anesthesia (20 mg/kg iv thiamylal sodium followed by 1% halothane) and aseptic conditions. The pursuit stimulus was a laser spot controlled by computer-driven mirror galvanometers that was back-projected onto a tangent screen 40 cm from the eyes. Eye position was monitored by a magnetic search coil system. Juice rewards were delivered by computer when the eye was within ±2° of the target for 500 ms.

RESULTS

Figure 5, *A* and *B*, shows results from simulations of the model during tracking along sum-of-two-sines and sum-of-three-sines trajectories. Corresponding data for a monkey tracking along the same trajectories are shown in Fig. 5, *C* and *D*, to the *right* of each model simulation. Both the model and the monkey showed excellent tracking performance along these complex target trajectories. For both the model simulations and the monkey experiments, sum-of-two-sines trajectories (V2H3 in Fig. 5, *A* and *C*) at a waveform (repeat) frequency of 0.30 Hz were created by summing an 0.6-Hz vertical sinusoid (V2) at 2 times the waveform frequency with an 0.9-Hz horizontal sinusoid (H3) at 3 times the waveform frequency of the trajectory. Similarly, sum-of-three-sines trajectories (H4H6V7 in Fig. 5, *B* and *D*) were created by summing three sinusoidal components, two horizontal (H4 and H6) and one vertical (V7), at frequencies 4, 6, and 7 times the waveform frequency of 0.15 Hz. The monkey tracking data were derived from our previously reported studies of component interactions during sum-of-sines pursuit (Kettner et al. 1996).

Figure 6 shows quantitative measurements of performance for model simulations (open symbols) in terms of component gains and phases (see METHODS). Six sets of data points correspond to results for six trajectories: the H3V2 and H4H6V7 trajectories displayed in Fig. 5 and the H2H3 trajectory (discussed in more detail below) presented at four waveform frequencies of 0.3, 0.4, 0.5, and 0.6 Hz. Thus three gain/phase points define tracking for the high-, middle-, and low-frequency components of the H4H6V7 waveform, and two gain/phase points define high- and low-frequency tracking for each of the other five sum-of-two-sines trajectories. For the model, the average gain for all trajectory components was 0.97, whereas the average phase magnitude (absolute value) was 8 ms.

For comparison purposes, gain/phase pairs for monkey tracking of sum-of-sines trajectories are also presented in Fig. 6. These data were used previously to study component interactions during sum-of-sines pursuit (Kettner et al. 1996). They have been reanalyzed here so that phase angles are now expressed as phase delays in milliseconds to allow comparisons with the feedback delays obtained from the perturbation experiments described below. The greater number of points associated with the monkey data is due to the larger number of stimulus trajectories and frequencies used to study the monkey: four sum-of-two-sines and four sum-of-three-sines trajectories were each studied at three waveform frequencies. For the monkey, the average gain for all trajectory components was 0.84, whereas the average phase magnitude (absolute value) was 20 ms. The model's performance is included in the wide range of behaviors observed for monkey, but its output is closer to optimal performance of zero phase and unity gain than is the monkey's performance.

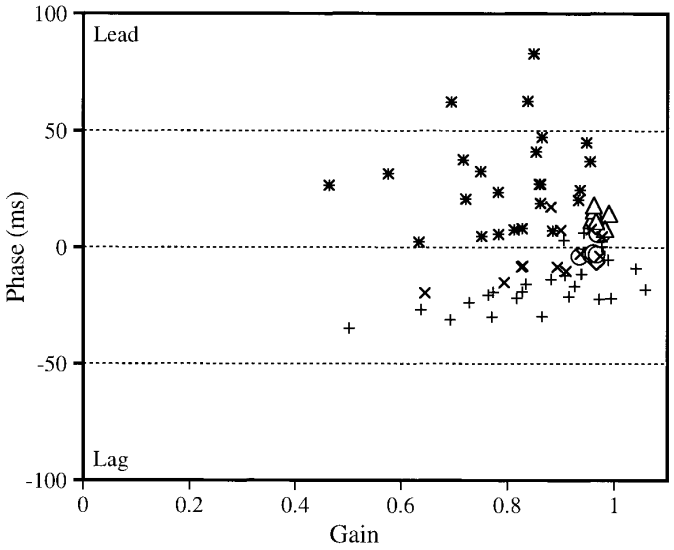

FIG. 6. Average component gain vs. phase values for the model and the monkey. In all instances, predictive pursuit is indicated by phases well in advance of the average visual feedback delays of 80 ms for the model and 90 ms for the monkey. Note that low-frequency components (represented by triangles for the model and asterisks for the monkey) were tracked with phase leads, whereas high-frequency components (represented by circles for the model and plus signs for the monkey) were tracked with phase lags. Open symbols: model performance. Other symbols: monkey behavior. High-, medium- (when present), and low-frequency component values are indicated for the model by circles, diamonds, and triangles, and for the monkey by plus signs, crosses, and asterisks, respectively. Model gain and phase values were based on performance along the H3V2 and H4H6V7 trajectories illustrated in Fig. 5 and the H2H3 trajectories used to study high- vs. low-frequency component tracking. Monkey gain and phase data were based on results reported in Kettner et al. (1996) and Leung and Kettner (1997) for 8 complex trajectories each at 3 waveform frequencies: H2H3, V2V3, H2V3, V2H3 (at 0.3, 0.4, and 0.5 Hz) and H4H6H7, V4V6V7, H4H6V7, V4V6H7 (at 0.05, 0.10, and 0.15 Hz). Here, for example, V4V6H7 indicates a combination of 2 vertical sinusoids and 1 horizontal sinusoid with frequencies 4, 6, and 7 times the waveform frequency, with each sinusoid in a waveform having the same average velocity. Each data point for the monkey data is based on performance during ≥100 waveform presentations (10 waveforms × 5 runs × 2 animals).

Interestingly, the model showed consistent differences in tracking phase for high- versus low-frequency components presented on the same axis: the high-frequency component was tracked with a phase lag, whereas the low-frequency component was tracked with a phase lead. For example, for the H4H6V7 trajectory, on the horizontal axis, the H4 trajectory was tracked with a phase lead of 14 ms, whereas the H6 trajectory was tracked with a phase lag of 6 ms; on the vertical axis, the V7 component was tracked with a phase lead of 6 ms. To further test this observation, we trained the model to track the sum-of-two-sines waveform H2H3 at four waveform frequencies of 0.3, 0.4, 0.5, and 0.6 Hz. Each of the H2H3 trajectories was created by summing a horizontal sinusoid (H2) at 2 times the waveform frequency with a horizontal sinusoid (H3) at 3 times the waveform frequency. Without exception, the higher-frequency H3 component was tracked with a phase lag (average lag = 3 ms), whereas the low-frequency H2 component was tracked with a phase lead (average lead = 14 ms). The model did not show this lag-lead effect for phase when components were separated on

horizontal and vertical axes. For the model, the tracking components for the V2H3 trajectory both showed phase leads (H3 lead = 8 ms; V2 lead = 6 ms). Similarly, the V7 component of the H4H6V7 waveform was tracked with a phase lead of 6 ms, even though it was the highest-frequency component, whereas the H6 and H4 components on the horizontal axis did follow the correct lag-lead relationship.

Similar results were obtained for our monkeys (Kettner et al. 1996). Notice in Fig. 6 that the high-frequency component phases (plus signs) for monkeys were associated with phase lags, whereas low-frequency components (asterisks) were always tracked with phase leads. Overall, the monkey tracked high-frequency components with an average phase lag of 8 ms, whereas low-frequency components were tracked with an average phase lead of 6 ms. Similar to the model, the monkey showed a weaker lag-lead relationship when component sinusoids were on opposite horizontal and vertical axes, but, unlike the model, this lag-lead relationship was still present. Although it is unclear why this difference between model and monkey performance occurs, it suggests that there is a greater separation between horizontal and vertical control for the model than for the monkey.

The model's response to an infrequent right-angle change in target trajectory (Fig. 7, *A* and *B*) was used to study its ability to respond to a perturbation during ongoing two-dimensional pursuit. Monkey tracking data from Leung and Kettner (1997) for the same trajectories are presented in Fig. 7, *C* and *D*. Here both the model and the monkey tracked a circular trajectory for three cycles before encountering a right-angle perturbation along a circle meridian on the fourth cycle. The model responded to unexpected perturbations in trajectory in much the same way the eye did. In Fig. 7*A* there is a continuation of the expected curved circular trajectory for about the same time period observed for the eye in Fig. 7*C*. Interestingly, the model had a somewhat stronger predictive component than the oculomotor system; it anticipated smoothly the abrupt change from an upward linear trajectory to the curved trajectory, whereas the eye stayed close to the upward path for a longer period of time. Unlike the eye, the model deviated slightly from the curved trajectory on those cycles when a perturbation did not occur.

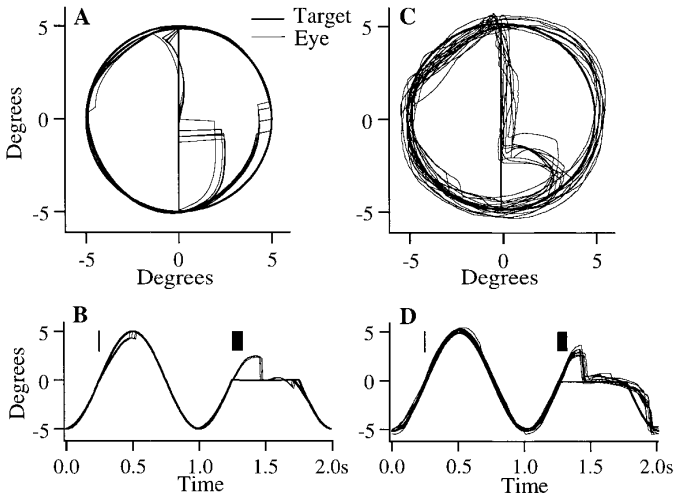

FIG. 7. Comparisons between model tracking (*A* and *B*) and monkey eye tracking (*C* and *D*) along perturbed trajectories. Heavy lines: target trajectories. Fine lines: tracking traces. *A* and *C*: average tracking of waveforms consisting of 3.5 cycles of a circular trajectory (1.0 Hz, 5°) followed by 0.5 cycle of vertical sinusoidal pursuit. After the perturbation, both eye and model followed the curvature of the expected circular trajectory before smooth and then saccadic corrections were made. *B* and *D*: individual horizontal position traces for the cycle before and during the perturbation. Bars above the nonperturbed cycle correspond to the small pursuit lags that are observed before perturbation, in comparison with the bars above the perturbed cycles, which indicate estimates of the much larger smooth correction latencies.

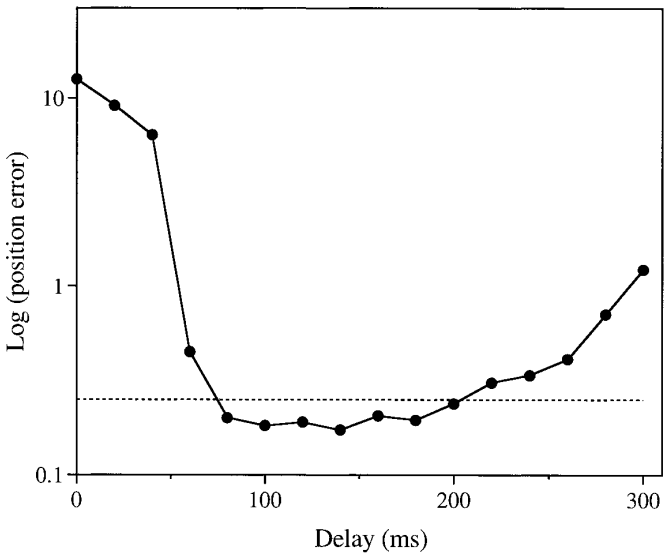

FIG. 8. Effects of the trace delay on model performance. Dotted line: saccade initiation error of 0.25°.

We used this perturbation paradigm to quantify delays in visual feedback, to compare these estimates with delays during smooth pursuit along the sum-of-sines trajectories described above, and to demonstrate the clear use of predictive control during by the model with the use of the same techniques used previously for the monkey (Leung and Kettner 1997). During circular pursuit before the perturbation, the model tracked the circle with average horizontal and vertical component gains of 0.95 and 1.00, and small average phase leads of 5 and 5 ms. These results compared well with average horizontal and vertical component gains of 0.96 and 0.84 and average phase lags of 4 and 2 ms for the monkey. In contrast to this excellent performance before the perturbation, the model showed visual feedback delays of 80 ms before it responded to the right-angle change in target direction after the perturbation. The monkey showed a similar average response latency of 90 ms. This indicates that there are limits to the tracking accuracy of the model that are similar to the limitations of the monkey pursuit system. Although the model was trained on the perturbation, it was not trained to produce the specific corrective response that was observed. Rather, the parameters of the model were constrained by physiological measurements and then trained to accurately match the perturbation trajectory, as indicated by a lack of retinal slip. Thus the model was trained to accurately respond to the right-angle perturbation but generated an overshoot similar to that exhibited by the eye.

The robustness of the model's learning rule was tested. For this purpose, the eligibility trace described in *Eq. 13* was used. This eligibility trace did not increase and decrease

gradually when the process modeled by *Eqs. 11* and *12* was used, but instead provided a record of parallel fiber input at the parallel-fiber-to-Purkinje-cell synapse that was simply delayed by *d* ms. This ''pure delay'' trace allowed us to systematically study the effects of trace delay on network learning. For each delay, the model was reset to the starting conditions defined in METHODS and trained for 50,000 simulated time steps. Results from this analysis (Fig. 8) indicate that this eligibility trace resulted in good model performance for delays that ranged from 80 to 200 ms. Here we measured model performance on the basis of the root-mean-square error during the final 4,000 time steps of the simulation and used an error criterion of 0.25° (Fig. 8, dotted line) to distinguish poor performance from good performance. This is the error level that the model uses to initiate a saccade that moves the eye back on target.

DISCUSSION

Previous models of predictive pursuit

In most previous models of smooth pursuit (e.g., Robinson et al. 1986; Young et al. 1968) it has been assumed that the system can be simulated with a small number of interconnected processing units that control eye movement by feedback/feedforward control. These models were designed primarily to explain pursuit along unpredictable target trajectories and to account for responses to trajectory steps. They also generate short-lag predictive tracking along straight-line constant-velocity ramp trajectories, because they are velocity controllers (Rashbass 1961; but see Pola and Wyatt 1980). After the eye has acquired the target, short-lag pursuit is maintained with a simple constant-velocity output.

However, the designers of these models stressed from the outset that they were not designed to generate predictive tracking along more complex trajectories including sinusoids that are tracked with little or no lag (Bahill and McDonald 1983; Dallos and Jones 1963; Lisberger et al. 1981). Here position, as well as velocity, acceleration, and the other, higher-order derivatives of sinusoidal motion varies continuously in time, and a constant controller output will not allow predictive tracking. One approach used to generate predictive tracking for sinusoidal target motions is to sum delayed position, velocity, and acceleration inputs to generate a sinusoidal control signal with a frequency equal to the common frequency of the inputs and a phase shift determined by the relative proportion of the inputs (Deno et al. 1995; Krauzlis and Lisberger 1989). For example, for sinusoidal motion both velocity and position vary sinusoidally with the same period, but with different phases: velocity is 90° ahead of position. Their combination (position + velocity) produces a sinusoid that has a frequency equal to shared frequency of the position and velocity components and a phase that is 45° ahead of position. In a similar fashion, other phase delays can be generated by varying the relative amplitudes of the position, velocity, and acceleration components. A suitable choice of these amplitudes can produce a control signal that compensates for some delays in visual feedback. Unfortunately, a particular choice of model parameters will only work for sinusoids with a single frequency. This approach will not work for sum-of-sines stimuli composed of different frequency sinusoids: a phase-shifted copy of a sum-of-sines waveform cannot be generated by summing position, velocity, and acceleration versions of that waveform.

To explain more complicated target motions, as well as sinusoidal pursuit, some investigators (e.g., Barnes and Asselman 1991; Van den Berg 1988) have suggested that the pursuit system has a buffer that stores the most recent cycle of a periodic target motion. If the next cycle is the same as the previous cycle, it is easy to see how this stored representation can be used to generate eye movements that predict target motion on the current cycle. Although this approach accounts for some experimental data, it is difficult to see how a buffer of this type would be implemented by a biological system. There are also problems in deciding what constitutes a cycle. For example, if a cycle transition is defined as a zero crossing, then it is difficult to determine where a complex waveform begins and ends. A related approach is to imagine that input signals are delayed by the repeat period of a complex waveform, but again, it is difficult to imagine how very long and accurate delays corresponding to long repeat periods would be produced by a biological system. For example, the ''fish'' trajectory described in the RESULTS section has a repeat period of 6.6 s.

Network model of smooth pursuit based on the cerebellum

The model of two-dimensional visual pursuit presented here is based rather directly on the anatomy and physiology of the flocculus and paraflocculus regions of the cerebellum. These areas are known to receive a rich diversity of visual, efference copy, and proprioceptive information via mossy fibers, and they send their Purkinje axons to brain stem nuclei known to control eye movements. Whereas previous pursuit models have utilized simplified representations of the visual- and movement-related signals, the present model uses 440 mossy fibers to simulate the rich diversity of mossy fiber latencies, directional tuning characteristics, and velocity and positional response properties that are observed experimentally (e.g., Miles et al. 1980). These mossy fiber input signals are combined randomly to generate an expansive recoding into 6,000 parallel fibers in the simulated granular layer.

It is then hypothesized that the Golgi cell system acts via a mechanism akin to lateral inhibition (see *Model*) to eliminate the activity for all but a subset of the most active granule cells during each time step. This process leads to a more sparse representation that improves the network's ability to distinguish input activity patterns. The result is a sparse expansive recoding that enhances the richness and discriminability of the vector of potential inputs (see Albus 1971; Marr 1969; Tyrrell and Willshaw 1992) that is furnished to Purkinje cells. It improves the probability that a predictable and unique relationship exists between the input vector and the desired response at any point in time, and this improves the likelihood that an adaptive solution will result from training. The range in latencies of mossy fiber input also enhances the likelihood of a solution, because it allows the dynamic properties of the pursuit task to be represented. The visual pathway samples diverse retinal signals that occurred 80–120 ms earlier, and the proprioceptive/efference copy path-

way samples diverse eye motion signals that occurred 0–40 ms earlier. With 6,000 different parallel fibers, the number of unique patterns of potential input is quite enormous, and the trajectories that are generated can be quite complex (see Fig. 5*B*).

The parallel fibers then synapse onto two Purkinje units: one that controls horizontal and another that controls vertical eye motion on the basis of the reported division of the flocculus into horizontal and vertical microzones (e.g., Sato and Kawasaki 1991). The Purkinje units generate eye motion via circuitry distinct from the cerebellar network. We follow the tradition that the cerebellar flocculus/parafloculus is one of several premotor structures generating eye velocity commands that converge on common brain stem circuitry that converts these commands into signals driving the extraocular muscles (see reviews by Fuchs et al. 1985; Robinson 1981a,b). We assume that premotor circuits in the brain stem perform ''neural integration'' (see Arnold and Robinson 1991; Robinson 1989) and saccade generation (e.g., Arai et al. 1994; Dean et al. 1994; Lefevre and Galiana 1992) and we model these functions with the use of simple equations. Thus we have not attempted to duplicate past modeling efforts that provide more detailed explanations of how these processes might be implemented. We have also restricted the scope of the model to the generation of eye movements when the head is fixed. In future work, we hope to account for vestibuloocular behaviors either via extensions of our cerebellar network or the incorporation of other network modeling results into the model (e.g., Anastasio and Robinson 1989).

Comparison between monkey and model performance

In this first study we chose to explore the model's ability to learn to track both the simple and more complex one- and two-dimensional target motions that have been the subject of recent experimental studies in our laboratory (Kettner et al. 1996; Leung and Kettner 1997). These experiments provide a good test of the model's capabilities because the monkeys' pursuit along these trajectories requires both predictive and feedback tracking, and this work is compatible with other studies of smooth pursuit (see INTRODUCTION). The model simulations produced results similar to the monkey data: the average phase difference between eye and target during complex sum-of-sines pursuit was 20 ms for the monkey and 8 ms for the model. These values were much shorter than response delays after right-angle changes in target direction during predictive circular pursuit, which averaged 90 ms for the monkey (Leung and Kettner 1997) and 80 ms for the model. Thus, for practiced target trajectories, both the monkey and the model can alter eye motion to follow a predictable target well before visual information about target motion can be processed by the pursuit system. The model also showed the lag-lead relationship that we (Kettner et al. 1995) and others (e.g., Barnes et al. 1987; Dallos and Jones 1963; Yasui and Young 1984) have observed for the high- versus low-frequency components of sum-of-sines trajectories when these components were on the same axis.

In addition, the model generated appropriate responses to perturbations from ongoing circular pursuit. The model's response to an abrupt freezing of horizontal target motion (bottom of the circle in Fig. 7*A*) is delayed by a visual reaction time. This is because the model's training experience consisted of a repeating trajectory that continued in its circular orbit in three of four cases. The occurrence of the perturbation was therefore not reliably predicted by visual signals 80–120 ms earlier, or by movement-related signals 0–40 ms earlier. The network was forced to rely on visual feedback that followed the perturbation by an average of 100 ms. In contrast, the subsequent resumption of horizontal target motion (top of the circle in Fig. 7*A*) followed the vertical segment of the target trajectory in all cases during training. Thus there was a reliable predictive relationship between parallel fiber activity and target trajectory that both the model and the monkey learned to exploit to reinitiate horizontal eye movement without having to rely on visual feedback.

Although the monkey behavior during perturbed circular pursuit is qualitatively similar to that of the model (Fig. 7), there are also differences. The model better anticipates the resumption of horizontal target motion at the top of the circle, and deviates from the circular trajectory during unperturbed cycles to a greater extent than the monkey. We conjecture that these and other differences can be explained by the much larger number of neurons in the monkey's cerebellar network, and its exposure to a much wider range of trajectories than the model. In terms of training time, the perturbation paradigm was one of the most difficult for the model to master, with a difficulty similar to the fish pattern (Fig. 5*B*). This is because the model had to learn two patterns, a circle and a half circle, and switch between the two at the point of perturbation. The difficult, but important, issue of how the model stores multiple trajectories and how it switches from one trajectory to another will provide one focus for future study. It should also be emphasized that the model does not include an explicit representation of the nonadaptive, feedback control systems hypothesized to exist by several researchers (e.g., Robinson et al. 1986; Young et al. 1968). This was done intentionally to determine how well the model would perform without them, but the addition of such a feedback loop external to our cerebellar network could improve the model's performance. Simultaneous control by several systems may correspond to what actually happens in the brain.

Learning mechanisms for credit assignment

The model incorporates a biologically motivated mechanism that allows it to adjust its weight parameters when new trajectories need to be learned. When one attempts to train a neural network with biologically reasonable signals, one is immediately confronted with two problems (Houk and Barto 1992; Sutton and Barto 1981). First, feedback related to the correctness of the behavioral response needs to be directed to those particular synapses that contribute to the response. This is referred to as the *structural* credit assignment problem. Second, there are significant delays between the synaptic events responsible for generating a command and the receipt of sensory signals that correspond to the resulting movement. The problem of compensating for this delay is called *temporal* credit assignment.

The learning mechanism utilized in the present model

addresses both of these credit assignment problems in a manner that is biologically motivated (see Houk and Alford 1996). The signal flow diagram in Fig. 9 summarizes our hypothesis of how this learning mechanism corresponds to cellular mechanisms for an individual parallel fiber, f_j, acting on a particular Purkinje cell, p_k. When the parallel fiber releases the neurotransmitter glutamate at the Purkinje cell's synaptic spine, the transmitter binds to two different types of glutamate receptors (Crepel and Krupa 1988; Ito 1989; Linden and Connor 1991), labeled mGlu and AMPA. The model assumes that this dual targeting of neurotransmitter sets in motion two distinct signaling processes, one that operates locally within the synaptic spine and another that contributes to the global function of the Purkinje cell (Houk et al. 1990).

The top part of the diagram summarizes the local process, held responsible for generating an eligibility trace (*Eq. 11* and *12*). The computational function of the eligibility trace is to preserve the recent history of how parallel fiber *j* has influenced Purkinje cell *k* sufficiently long to facilitate learning based on delayed training information. There are 12,000 (6,000 parallel fibers synapse on each of 2 Purkinje units) eligibility traces in the model, one for each synaptic spine, and this facilitates structural as well as temporal credit assignment. We assume that the eligibility process is kept local through the activation of the metabotropic class of glutamate receptors (mGlu). Through a G protein-mediated IP_3 (inositol-1,4,5-trisphosphate) reaction in the postsynaptic membrane, mGlu binding leads to the production of diacylglycerol (Crepel et al. 1996; Linden and Connor 1991). The latter substance is a cofactor, along with calcium, for the activation of PKC (Nishizuka 1986). Although the precise time course of this reaction in the spines is not known, the fact that it works through G proteins means that it will be slow in comparison with direct activation of Purkinje cells by ionic current. We have modeled the kinetics of this reaction as a simple first-order process leading to the active form of PKC labeled q_{jk} in Fig. 9. Another first-order process is used to model the kinetics of AMPA receptor phosphorylation by activated PKC labeled r_{jk} in Fig. 9. Phosphorylation of the AMPA receptor (AMPA~P) causes a desensitization that is related to LTD (Hemart et al. 1994; Ito and Karachot 1992). Because AMPA~P tends to be dephosphorylated by another enzyme, called phosphatase, the consolidation of receptor desensitization into a lasting long-term depression (LTD) probably requires another cellular process, the protein kinase G step (Crepel et al. 1996), which is discussed below. We equate LTD with the weight change, Δw_{jk}, at spine jk.

The bottom part of the signal flow diagram (Fig. 9) summarizes the global process of synaptic integration that leads to eye movement control. Through the existing weight w_{jk}, parallel fiber f_j has a nearly immediate influence on the electrical activity of Purkinje cell p_k. This fast synaptic current is mediated by ionotropic AMPA receptors (Ito 1989). The current spreads from the spine to the soma of the Purkinje cell, where it summates with synaptic currents produced by other parallel fibers, ultimately determining the activity level p_k of the Purkinje cell. The latter contributes to the generation of a motor command calling for an eye movement x_k in plane k. Purkinje cells controlling horizontal and vertical eye movements are segregated into horizontal and vertical zones that are innervated by climbing fibers (c_k) sensitive to retinal errors in the same plane controlled by the Purkinje cell (Sato and Kawasaki 1991). This specific connectivity contributes to structural credit assignment because the correctness of the movement in, for example, the horizontal plane is evaluated by a climbing fiber response related to errors in the horizontal plane.

Recall that the functional role of the eligibility trace in the model is to compensate for the 100-ms delay between Purkinje cell activity and the climbing fiber activity that provides training information relevant to that activity. We selected the time constants of the PKC and AMPA~P processes so that the eligibility traces peak at ~100 ms and decay slowly thereafter (Fig. 4). This ensures that synaptic events that occurred considerably in advance of the climbing fiber response are well represented by the phosphorylation state of the AMPA receptor, r_{jk}. The model assumes that another cellular process is available to translate r_{jk} into the weight change Δw_{jk}. A signal transduction cascade that involves nitric oxide and protein kinase G has been implicated as a mechanism for inhibiting the phosphatase (Crepel et al. 1996; Lev-Ram et al. 1995), which could serve to translate eligibility into a weight change (Houk and Alford 1996). *Equation 14* is used to model this memory consolidation step.

From a computational standpoint, the important features

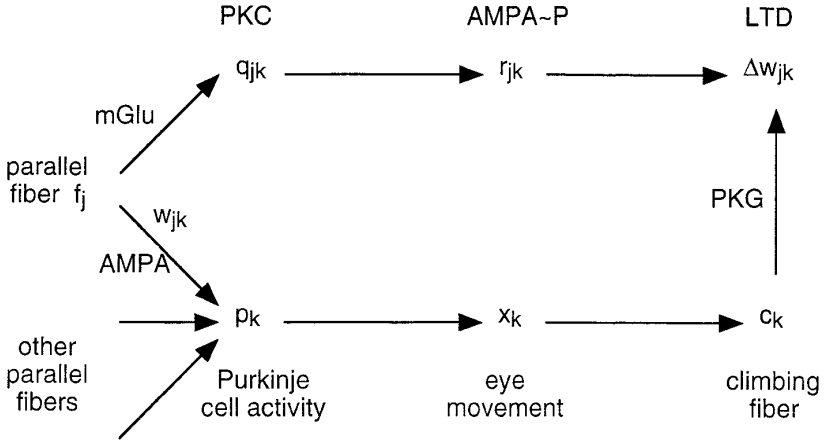

FIG. 9. Diagram illustrating a possible neural substrate for the eligibility trace as explained in the DISCUSSION section.

of these processes are *1*) the use of local eligibility traces that preserve the recent history of activity in each synaptic spine and *2*) a mechanism for translating these local signals into long-lasting changes in synaptic weight on the receipt of error information that is inevitably delayed. These processes are biologically plausible, on the basis of current knowledge of the signal transduction mechanisms that underlie LTP. Alternative mechanisms of plastic neural change, such as synaptogenesis (Weiler et al. 1994), could serve equally well, provided they have computational features that are capable of resolving the temporal and structural credit assignment problems.

Experimental support for an eligibility mechanism

The eligibility trace is a necessary feature of our model. When we attempted to train a version of the model that lacked an eligibility trace, the model was not able to learn predictive tracking. In contrast, accurate learning occurred with pure delay eligibility traces when the relative timing of parallel fiber and climbing fiber activity ranged from 80 to 200 ms, with reduced accuracy for shorter and longer delays. Before these simulations were run, we had predicted that the optimal delay for learning would be 100 ms, the delay that exactly compensated for the model's climbing fiber delay of 100 ms. Surprisingly, although the range of delays that allowed accurate learning included 100 ms, this range was not centered on 100 ms: five delays >100 ms led to accurate learning, but only a single delay <100 ms worked. We are not sure why this asymmetry with respect to the optimal delay was produced. We conjecture that it is due to an interaction between the model's generation of corrective saccades after retinal errors and its eligibility mechanism.

Only a few biological experiments have been designed to test the effects of different timing intervals between parallel and climbing fiber activations on the induction of LTD. Recently, in support of our learning rule, Chen and Thompson (1995) found that LTD is strongest when parallel fibers are activated 125–250 ms before climbing fibers in rabbit cerebellar slices. In other recent experiments based on patch recordings in rabbit cerebellar slices, Schreurs et al. (1996) have shown pairing-specific LTD when parallel fiber activation preceded climbing fiber activation by 80 ms with 30- to 40-s intertrial intervals. Somewhat different results had been reported in previous experiments (Ito et al. 1982; Kano and Kato 1988) that demonstrated LTD in the cerebellar slice with the use of simultaneous activation of parallel and climbing fibers, or when climbing fiber activation preceded parallel fiber activation. These differences may be due to differences in experimental procedure. For instance, past studies showed LTD with the application of γ-aminobutyric acid blockers such as bicuculline, which were not required in the experiments of Chen and Thompson (1995) and Schreurs et al. (1996). In addition, earlier studies used relatively short interstimulus intervals that did not allow clear distinctions between lags and leads during alternate stimulation of parallel and climbing fibers. Thus, for a typical repeat period of 250 ms (4 Hz), a parallel fiber lag of 20 ms was equivalent to a parallel fiber lead of 230 ms, making it difficult to establish whether the short lag or the longer lead was the important variable controlling LTD. The longer repeat periods used by Chen and Thompson (1995) and Schreurs et al. (1996) allow clearer distinctions between leads and lags. It is also possible that more than a single cellular mechanism controls synaptic depression (see Schreurs et al. 1996).

Comparisons with other models

This model adds to, rather than replaces, existing models of oculomotor performance. It works in concert with other systems that produce neural integration, saccade generation, and vestibular control. The model's primary contribution is the addition of a biologically feasible way of generating predictive control, but, to do so, it draws on several concepts previously used to model prediction. It resembles most models in its use of input signals related to the derivatives (position, velocity, and acceleration) of eye and target motion, but is considerably more complex than models that sum simple combinations of these variables (Deno et al. 1995; Krauzlis and Lisberger 1989). Initial versions of the network model with fewer parallel fibers did not learn complex trajectories. On the basis of physiological data, the model uses mossy fiber inputs that are delayed by a range of 0–40 ms for eye motion and 80–120 ms for visual motion. These delays can be thought of as corresponding to a large number of short-term buffers or short-delay lines that maintain information until it is used to generate pursuit. However, these inputs can only hold a small part (no more than 120 ms) of a periodic waveform and therefore cannot generate predictive pursuit in the straightforward fashion envisioned by some buffer models (see above).

Several other models of motor control have been linked to the cerebellum with varying degrees of correspondence between model and physiology (see the review by Houk et al. 1996). The classic work of Marr (1969) and Albus (1971) suggested that the cerebellum played a role in pattern recognition, and learned with the use of climbing fiber signals. Marr suggested that the cerebellum translates input contexts into elemental output movements. Albus postulated that the cerebellum was equivalent to the classical Perceptron pattern classification device (Rosenblatt 1961) and suggested that feedback from one movement could generate the next command in a sequence of muscle commands. Our model extends this work to allow the control of continuous predictive movement with the use of a model structure with realistic delays. Fujita (1982a,b) suggested a role for the cerebellum as an adaptive filter in which Purkinje cells weighted contributions from a series of linear filters. Here each linear filter was implemented by networks of Golgi and granule units. Fujita's model generates pursuit along sinusoidal trajectories, but has not been tested for more complex trajectories. Its use of granule and Golgi units as linear filters differs from our use of these elements to improve pattern recognition via sparse expansive recoding of mossy fibers inputs. The idea that the cerebellum is involved in timing or prediction has been proposed by several investigators of classical conditioning (Bartha et al. 1991; Buonomano and Mauk 1994; Moore and Blazis 1989; Moore et al. 1989) and general motor control (Braitenberg 1967, 1987; Freeman 1969; Ito 1984; Keeler 1990; Miall et al. 1993;

Pellionisz and Llinas 1979). Our model also resembles several cerebellar models proposed by Kawato and colleagues (Gomi and Kawato 1992; Kawato and Gomi 1992) that emphasize feedback error learning, the need for predictive control, and some correspondence with cerebellar anatomy. These models differ from our models in some ways: we use sensory error climbing fiber signals instead of motor error as training signals, and we do not assume explicit representations of the trajectory and an inverse model of the plant (Barto et al. 1996; Berthier et al. 1993) (present model). This is not to suggest that the two approaches are incompatible. For the relatively simple oculomotor plant, sensory and motor errors are more closely related than in other systems. It is also inevitable that our models develop at least an implicit representation of the inverse plant to allow correct outputs via the plant. The present model does emphasize, more strongly than any of these models, the need to incorporate realistic mossy and climbing fiber delays and tuning functions, along with a training rule that uses a delayed eligibility trace.

The present model bears a close functional relationship to certain mathematical techniques for nonlinear adaptive predictive control (Astrom and Wittenmark 1995; Goodwin and Sin 1984) that have been used to control dynamic systems on the basis of delayed inputs. These techniques convert a vector of input values distributed over a range of time delays into a desired output vector with the use of a transformation matrix. In our model, the parallel fiber activation pattern corresponds to the input vector, the parallel-fiber-to-Purkinje-cell weights correspond to the values of the transformation matrix, and the output vector is represented by the activities of the Purkinje cells. These systems typically utilize input information that arrives over a range of delays. This corresponds to the distributions of delays observed for the different mossy fiber inputs in the model (Miles et al. 1980). Here is an example of where the response diversity that is frequently associated with the nervous system may facilitate the computation of upcoming target direction. Correspondences between this powerful class of nonlinear adaptive predictive controllers and the view of cerebellar function presented here suggests how the cerebellum could generate complex motor output.

This work was supported by National Institutes of Health Grants P50 MH-48185 and T32 DC-00015-13.

Address for reprint requests: R. E. Kettner, Dept. of Physiology M211, Northwestern University Medical School, 303 E. Chicago Ave., Chicago, IL 60611.

Received 30 August 1996; accepted in final form 18 December 1996.

REFERENCES

ALBUS, J. S. A theory of cerebellar function. *Math. Biosci.* 10: 25–61, 1971.

ANASTASIO, T. J. AND ROBINSON, D. A. The distributed representation of vestibulo-oculomotor signals by brain-stem neurons. *Biol. Cybern.* 61: 79–88, 1989.

ARAI, K., KELLER, E. L., AND EDELMAN, J. A. Two-dimensional neural network model of the primate saccadic system. *Neural Networks* 7: 1115–1135, 1994.

ARNOLD, D. B. AND ROBINSON, D. A. A learning network model of the neural integrator of the oculomotor system. *Biol. Cybern.* 64: 447–454, 1991.

ASTROM, K. J. AND WITTENMARK, B. *Adaptive Control.* Menlo Park, CA: Addison-Wesley, 1995.

BAHILL, A. T. AND MCDONALD, J. D. Smooth pursuit eye movements in response to predictable target motions. *Vision Res.* 23: 1573–1583, 1983.

BARNES, G. R. AND ASSELMAN, P. T. The mechanism of prediction in human smooth pursuit eye movements. *J. Physiol. Lond.* 439: 439–461, 1991.

BARNES, G. R., DONNELLY, S. F., AND EASON, R. D. Predictive velocity estimation in the pursuit reflex response to pseudo-random and step displacement stimuli in man. *J. Physiol. Lond.* 389: 111–136, 1987.

BARTHA, G. T., THOMPSON, R. F., AND GLUCK, M. A. Sensorimotor learning and the cerebellum. In: *Visual Structures and Integrated Functions,* edited by M. A. Arbib and J. Ewert. Berlin: Springer-Verlag, 1991, p. 381–396.

BARTO, A. G., BUCKINGHAM, J. T., AND HOUK, J. C. A predictive switching model of cerebellar movement control. In: *Advances in Neural Information Processing Systems 8,* edited by D. S. Touretzky, M. C. Mozer, and M. E. Hasselmo. Cambridge, MA: MIT Press, 1996, p. 138–144.

BECKER, W. AND FUCHS, A. F. Prediction in the oculomotor system: smooth pursuit during transient disappearance of a visual target. *Exp. Brain Res.* 57: 562–575, 1984.

BERTHIER, N. E., SINGH, S. P., BARTO, A. G., AND HOUK, J. C. Distributed representation of limb motor programs in arrays of adjustable pattern generators. *J. Cognit. Neurosci.* 5: 56–78, 1993.

BRAITENBERG, V. Is the cerebellar cortex a biological clock in the millisecond range? *Prog. Brain Res.* 25: 334–336, 1967.

BRAITENBERG, V. The cerebellum and the physics of movement: some speculations. In: *Cerebellum and Neuronal Plasticity,* edited by M. Glickstein, C. Yeo, and J. Stein. New York: Plenum, 1987, p. 193–207.

BUCKINGHAM, J. T., BARTO, A. G., AND HOUK, J. C. Adaptive predictive control with a cerebellar model. In: *Proceedings of the 1995 World Congress on Neural Networks.* Hillsdale, NJ: Erlbaum, 1995, p. 373–380.

BUONOMANO, D. V. AND MAUK, M. D. Neural network model of the cerebellum: temporal discrimination and the timing of motor responses. *Neural Comput.* 6: 38–55, 1994.

CARL, J. R. AND GELLMAN, R. S. Adaptive responses in human smooth pursuit. In: *Adaptive Processes in Visual and Oculomotor Systems,* edited by E. L. Keller and D. S. Zee. Oxford, UK: Pergamon, 1986, p. 335–339.

CHEN, C. AND THOMPSON, R. F. Temporal specificity of long-term depression in parallel fiber–Purkinje synapses in rat cerebellar slice. *Learn. Memory* 2: 185–198, 1995.

COLLEWIJN, H. AND TAMMINGA, E. P. Human smooth and saccadic eye movements during voluntary pursuit of different target motions on different backgrounds. *J. Physiol. Lond.* 351: 217–250, 1984.

CREPEL, F., HEMART, N., JAILLARD, D., AND DANIEL, H. Cellular mechanisms of long-term depression in the cerebellum. *Behav. Brain Sci.* 19: 347–353, 1996.

CREPEL, F. AND KRUPA, M. Activation of protein kinase C induces a long term depression of glutamate sensitivity of cerebellar Purkinje cells. An in vitro study. *Brain Res.* 458: 397–401, 1988.

DALLOS, P. J. AND JONES, R. W. Learning behavior of the eye fixation control system. *IEEE Trans. Automatic Control* 8: 218–227, 1963.

DEAN, P., MAYHEW, J. E., AND LANGDON, P. Learning and maintaining saccadic accuracy: a model of brainstem-cerebellar interactions. *J. Cognit. Neurosci.* 6: 117–138, 1994.

DENO, D. C., CRANDALL, W. F., SHERMAN, K., AND KELLER, E. L. Characterization of prediction in the primate visual smooth pursuit system. *Biosystems* 34: 107–128, 1995.

FREEMAN, J. A. The cerebellum as a timing device: an experimental study in the frog. In: *Neurobiology of Cerebellar Evolution and Development,* edited by R. Llinas. Chicago, IL: AMA, 1969, p. 397–420.

FUCHS, A. F. Saccadic and smooth pursuit eye movements in the monkey. *J. Physiol. Lond.* 191: 609–631, 1967.

FUCHS, A. F., KANEKO, C.R.S., AND SCUDDER, C. A. Brainstem control of saccadic eye movements. *Annu. Rev. Neurosci.* 8: 307–337, 1985.

FUJITA, M. Adaptive filter model of the cerebellum. *Biol. Cybern.* 45: 195–206, 1982a.

FUJITA, M. Simulation of adaptive modification of the vestibulo-ocular reflex with an adaptive filter model of the cerebellum. *Biol. Cybern.* 45: 207–214, 1982b.

FUKUSHIMA, K., KANEKO, C. R., AND FUCHS, A. F. The neuronal substrate of integration in the oculomotor system. *Prog. Neurobiol.* 39: 609–639, 1992.

GOMI, H. AND KAWATO, M. Adaptive feedback control models of the vetibulocerebellum and spinocerebellum. *Biol. Cybern.* 68: 105–114, 1992.

GOODWIN, G. C. AND SIN, K. S. *Adaptive Filtering Prediction and Control.* Englewood Cliffs, NJ: Prentice-Hall, 1984.

HEMART, N., DANIEL, H., JAILLARD, D., AND CREPEL, F. Properties of glutamate receptors are modified during long-term depression in cerebellar Purkinje cells. *Neurosci. Res.* 19: 213–221, 1994.

HOUK, J. C. AND ALFORD, S. Computational significance of the cerebellar mechanisms for synaptic plasticity in Purkinje cells. *Behav. Brain Sci.* 19: 457–461, 1996.

HOUK, J. C. AND BARTO, A. G. Distributed sensorimotor learning. In: *Tutorials in Motor Behavior*, edited by G. E. Stelmach and J. Requin. Amsterdam: Elsevier, 1992, vol. II, p. 77–100.

HOUK, J. C., BUCKINGHAM, J. T., AND BARTO, A. G. Models of the cerebellum and motor learning. *Behav. Brain Sci.* 19: 368–383, 1996.

HOUK, J. C., SINGH, S. P., FISHER, C., AND BARTO, A. G. An adaptive sensorimotor network inspired by the anatomy and physiology of the cerebellum. In: *Neural Networks for Control*, edited by W. T. Miller, R. S. Sutton, and P. J. Werbos. Cambridge, MA: MIT Press, 1990, p. 301–348.

ITO, M. *The Cerebellum and Neuronal Control.* New York: Raven, 1984.

ITO, M. Long term depression. *Annu. Rev. Neurosci.* 12: 85–102, 1989.

ITO, M. AND KARACHOT, L. Protein kinases and phosphatase inhibitors mediating long-term desensitization of glutamate receptors in cerebellar Purkinje cells. *Neurosci. Res.* 14: 27–38, 1992.

ITO, M., SAKURAI, M., AND TONGROACH, P. Climbing fibre induced depression of both mossy fibre responsiveness and glutamate sensitivity of cerebellar Purkinje cells. *J. Physiol. Lond.* 324: 113–134, 1982.

KANO, M. AND KATO, M. Mode of induction of long-term depression at parallel fibre–Purkinje cell synapses in rabbit cerebellar cortex. *Neurosci. Res.* 5: 544–556, 1988.

KAWATO, M. AND GOMI, H. A computational model of four regions of the cerebellum based on feedback-error learning. *Biol. Cybern.* 68: 95–103, 1992.

KEELER, J. D. A dynamical system view of cerebellar function. *Physica D* 42: 396–410, 1990.

KELLER, E. L. Accommodative vergence in the alert monkey. *Vision Res.* 13: 1565–1575, 1973.

KETTNER, R. E., LEUNG, H.-C., AND PETERSON, B. W. Predictive smooth pursuit of complex two-dimensional trajectories in monkey: component interactions. *Exp. Brain Res.* 108: 221–235, 1996.

KETTNER, R. E., MAHAMUD, S., LEUNG, H.-C., BARTO, A. G., HOUK, J. C., AND PETERSON, B. W. Predictive smooth pursuit eye movements are generated by a cerebellar model, *Soc. Neurosci. Abstr.* 21: 520, 1995.

KLOPF, A. H. *Brain Function and Adaptive Systems—A Heterostatic Theory.* Bedford, MA: Air Force Cambridge Research Laboratories, 1972, AFCRL-72-0164.

KLOPF, A. H. *The Hedonistic Neuron: A Theory of Memory, Learning, and Intelligence.* Washington, DC: Hemisphere, 1982.

KOWLER, E. AND STEINMAN, R. M. The effect of expectations on slow oculomotor control. I. Periodic target steps. *Vision Res.* 19: 619–632, 1979.

KRAUZLIS, R. J. AND LISBERGER, S. G. A control systems model of smooth pursuit eye movements with realistic emergent properties. *Neural Comput.* 1: 116–122, 1989.

LEFEVRE, P. AND GALIANA, H. L. Dynamic feedback to the superior colliculus in a neural network model of the gaze control system. *Neural Networks* 5: 871–890, 1992.

LEUNG, H.-C. AND KETTNER, R. E. Predictive smooth pursuit of complex two-dimensional trajectories demonstrated by perturbation responses in monkeys. *Vision Res.* In press.

LEV-RAM, V., MAKINGS, L. R., KEITZ, P. F., KAO, J.P.Y., AND TSIEN, R. Y. Long-term depression in cerebellar Purkinje neurons results from coincidence of nitric oxide and depolarization-induced Ca^{2+} transients. *Neuron* 15: 407–415, 1995.

LINDEN, D. J. AND CONNOR, J. A. Participation of postsynaptic PKC in cerebellar long-term depression in culture. *Science Wash. DC* 254: 1656–1659, 1991.

LISBERGER, S. G., EVINGER, C., JOHANSON, G. W., AND FUCHS, A. F. Relationship between acceleration and retinal image velocity during foveal smooth pursuit in man and monkey. *J. Neurophysiol.* 46: 229–249, 1981.

LISBERGER, S. G. AND FUCHS, A. F. Role of primate flocculus during rapid behavioral modification of vestibuloocular reflex. I. Purkinje cell activity during visually guided horizontal smooth-pursuit eye movements and passive head rotation. *J. Neurophysiol.* 41: 733–763, 1978a.

LISBERGER, S. G. AND FUCHS, A. F. Role of primate flocculus during rapid behavioral modification of vestibuloocular reflex. II. Mossy fiber firing patterns during horizontal head rotation and eye movement. *J. Neurophysiol.* 41: 764–777, 1978b.

LISBERGER, S. G. AND WESTBROOK, L. E. Properties of visual inputs that initiate horizontal smooth pursuit eye movements in monkeys. *J. Neurosci.* 5: 1662–1673, 1985.

MAEKAWA, K. AND KIMURA, M. Mossy fiber projections to the cerebellar flocculus from the extraocular muscle afferents. *Brain Res.* 191: 313–325, 1980.

MAHAMUD, S. *A Model of Prediction in the Smooth Pursuit System* (Masters thesis). Amherst, MA: Univ. of Massachusetts, 1995.

MAHAMUD, S., BARTO, A. G., KETTNER, R. E., AND HOUK, J. C. A model of prediction in smooth eye movements. In: *Computational Neuroscience*, edited by J. M. Bower. New York: Academic, 1996, p. 379–384.

MARR, D. A theory of cerebellar cortex. *J. Physiol. Lond.* 202: 437–470, 1969.

MIALL, R. C., WEIR, D. J., WOLPERT, D. M., AND STEIN, J. F. Is the cerebellum a smith predictor? *J. Mot. Behav.* 25: 203–216, 1993.

MILES, F. A., FULLER, J. H., BRAITMAN, D. J., AND DOW, B. M. Long-term adaptive changes in primate vestibuloocular reflex. III. Electrophysiological observations in flocculus of normal monkeys. *J. Neurophysiol.* 43: 1437–1476, 1980.

MOORE, J. W. AND BLAZIS, D. E. J. Simulation of a classically conditioned response: a cerebellar implementation of the Sutton-Barto-Desmond model. In: *Neural Models of Plasticity*, edited by J. H. Byrne and W. O. Berry. San Diego, CA: Academic, 1989, p. 187–207.

MOORE, J. W., DESMOND, J. E., AND BERTHIER, N. E. Adaptively timed conditioned responses and the cerebellum: a neural network approach. *Biol. Cybern.* 62: 17–28, 1989.

MUSTARI, M. J., FUCHS, A. F., AND WALLMAN, J. Response properties of dorsolateral pontine units during smooth pursuit in the rhesus monkey. *J. Neurophysiol.* 60: 664–686, 1988.

NISHIZUKA, Y. Studies and perspectives of protein kinase C. *Science Wash. DC* 233: 305–311, 1986.

PALKOVITS, M., MAGYAR, P., AND SZENTAGOTHAI, J. Quantitative histological analysis of the cerebellar cortex in the cat. IV. Mossy fiber–Purkinje cell numerical transfer. *Brain Res.* 45: 15–29, 1972.

PELLIONISZ, A. AND LLINAS, R. Brain modeling by tensor network theory and computer simulation. The cerebellum: distributed processor for predictive coordination. *Neuroscience* 4: 323–348, 1979.

POLA, J. AND WYATT, H. Target position and velocity: the stimuli for smooth pursuit eye movements. *Vision Res.* 20: 523–534, 1980.

PRESS, W. H., TEUKOLSKY, S. A., VETTERLING, W. T., AND FLANNERY, B. P. *Numerical Recipes in C: The Art of Scientific Computing* (2nd ed.). Cambridge, UK: Cambridge Univ. Press, 1992.

RASHBASS, C. The relationship between saccadic and smooth tracking eye movements. *J. Physiol. Lond.* 159: 326–338, 1961.

ROBINSON, D. A. The mechanics of human smooth pursuit eye movements. *J. Physiol. Lond.* 180: 569–591, 1965.

ROBINSON, D. A. Control of eye movements. In: *Handbook of Physiology. The Nervous System. Motor Control.* Bethesda, MD: Am. Physiol. Soc., 1981a, sect. 1, vol. II, p. 1275–1320.

ROBINSON, D. A. The use of control systems analysis in the neurophysiology of eye movements. *Annu. Rev. Neurosci.* 4: 463–503, 1981b.

ROBINSON, D. A. Integrating with neurons. *Annu. Rev. Neurosci.* 12: 33–45, 1989.

ROBINSON, D. A., GORDON, J. L., AND GORDON, S. E. A model of the smooth pursuit eye movement system. *Biol. Cybern.* 55: 43–57, 1986.

ROSENBLATT, F. *Principles of Neurodynamics: Perceptrons and the Theory of Brain Mechanisms.* Washington, DC: Spartan, 1961.

SATO, Y. AND KAWASAKI, T. Identification of the Purkinje cell/climbing fiber zone and its target neurons responsible for eye-movement control by the cerebellar flocculus. *Brain Res. Rev.* 16: 39–64, 1991.

SCHREURS, B. G., OH, M. M., AND ALKON, D. L. Pairing-specific long-term depression of Purkinje cell excitatory postsynaptic potentials results from a classical conditioning procedure in the rabbit cerebellar slice. *J. Neurophysiol.* 75: 1051–1060, 1996.

STONE, L. S. AND LISBERGER, S. G. Visual responses of Purkinje cells in the cerebellar flocculus during smooth pursuit eye movements in monkeys. I. Simple spikes. *J. Neurophysiol.* 63: 1241–1261, 1990a.

STONE, L. S. AND LISBERGER, S. G. Visual responses of Purkinje cells in the

cerebellar flocculus during smooth pursuit eye movements in monkeys. II. Complex spikes. *J. Neurophysiol.* 63: 1262–1275, 1990b.

SUTTON, R. S. AND BARTO, A. G. Toward a modern theory of adaptive networks: expectation and prediction. *Psychol. Rev.* 88: 135–170, 1981.

SUZUKI, D. A., MAY, J. G., KELLER, E. L., AND YEE, R. D. Visual motion response properties of neurons in dorsolateral pontine nucleus of alert monkey. *J. Neurophysiol.* 63: 37–59, 1990.

TYRRELL, T. AND WILLSHAW, D. J. Cerebellar cortex: its simulation and the relevance of Marr's theory. *Proc. R. Soc. Lond. B Biol. Sci.* 336: 239–257, 1992.

VAN DEN BERG, A. V. Human smooth pursuit during transient perturbations of predictable and unpredictable target movement. *Exp. Brain Res.* 72: 95–108, 1988.

WEILER, I. J., WANG, X., AND GREENOUGH, W. T. Synapse-activated protein synthesis as a possible mechanism of plastic neural change. *Prog. Brain Res.* 100: 189–194, 1994.

YASUI, S. AND YOUNG, L. R. On the predictive control of foveal eye tracking and slow phases of optokinetic and vestibular nystagmus. *J. Physiol. Lond.* 347: 17–33, 1984.

YOUNG, L. R., FORSTER, J. D., AND VAN HOUTTE, N. A revised stochastic sampled data model for eye tracking movements. In: *Annual Conference on Manual Control (NASA SP-192)*. Washington, DC: Government Printing Office, 1968, p. 489–508.

ZEE, D. S., ATSUMI, Y., BUTLER, P. H., AND GÜÇER, G. Effects of ablation of flocculus and paraflocculus on eye movements in primate. *J. Neurophysiol.* 46: 878–899, 1981.